

3-D feature of self-correlation level contours at 10^{10} cm scale in solar wind turbulence

HONGHONG WU,¹ CHUANYI TU,¹ XIN WANG,² JIANSEN HE,¹ AND LINGHUA WANG¹

¹*School of Earth and Space Sciences, Peking University, Beijing, People's Republic of China*

²*School of Space and Environment, Beihang University, Beijing, People's Republic of China*

Submitted to ApJ

ABSTRACT

The self-correlation level contours at 10^{10} cm scale reveal a 2-D isotropic feature in both the slow solar wind fluctuations and the fast solar wind fluctuations. However, this 2-D isotropic feature is obtained based on the assumption of axisymmetry with respect to the mean magnetic field. Whether the self-correlation level contours are still 3-D isotropic remains unknown. Here we perform for the first time a 3-D self-correlation level contours analysis on the solar wind turbulence. We construct a 3-D coordinate system based on the mean magnetic field direction and the maximum fluctuation direction identified by the minimum-variance analysis (MVA) method. We use data with 1-hour intervals observed by WIND spacecraft from 2005 to 2018. We find, on one hand, in the slow solar wind, the self-correlation level contour surfaces for both the magnetic field and the velocity field are almost spherical, which indicates a 3-D isotropic feature. On the other hand, there is a weak elongation in one of the perpendicular direction in the fast solar wind fluctuations. The 3-D feature of the self-correlation level contours surfaces cannot be explained by the existed theory.

Keywords: solar wind, turbulence, magnetic fields, plasmas

1. INTRODUCTION

The magnetohydrodynamic (MHD) turbulence exhibits anisotropic features as a result of the preferred direction that the background magnetic field determines (Shebalin et al. 1983). The solar wind is observed to be in a turbulence state (Tu & Marsch 1995) and various studies proposed that solar wind turbulence is 2-D anisotropic based on theories (Oughton et al. 1994; Goldreich & Sridhar 1995), simulations (Cho & Vishniac 2000) and observations related to the power spectral index (Horbury et al. 2008; Podesta 2009; Chen et al. 2010; Wicks et al. 2010; He et al. 2013), structure function (Luo & Wu 2010) and correlation function (Matthaeus et al. 1990; Dasso et al. 2005).

The Maltese cross is one 2-D pioneering work. It consists of two lobes, one elongated along to the mean field direction (slab-like fluctuations), and the other elongated along the perpendicular direction to the mean field direction (2-D fluctuations) and is obtained by a 2-D self-correlation analysis (Matthaeus et al. 1990). Dasso et al. (2005) applied the correlation function method by using two-day-long data from Advanced Composition Explorer (ACE) spacecraft for the slow solar wind and the fast solar wind separately. They find that the fast wind mainly contains slab-like fluctuations and the slow wind 2-D fluctuations. However, Wang et al. (2019) find that the self-correlation function level contours of the magnetic field and the velocity field are 2-D isotropic for both the slow solar wind and the fast solar wind at 10^{10} cm scale using the same method as Dasso et al. (2005).

The 2-D anisotropic studies have been extended to the 3-D scenario which includes not only the mean magnetic field direction, but also the perpendicular magnetic field fluctuation direction. Boldyrev (2006) predicted theoretically that the solar wind turbulence is 3-D anisotropic with $l_{\parallel} > l_{\perp 2} > l_{\perp 1}$, where l_{\parallel} , $l_{\perp 2}$, $l_{\perp 1}$ are correlation lengths in the mean magnetic field direction, the perpendicular magnetic field fluctuation direction and the direction perpendicular to both, respectively. Chen et al. (2012) used the local structure function method to analyze the 3-D structure of turbulence

in the fast solar wind in a new local coordinate system from the outer scale to the proton gyroscale. Verdini et al. (2018) used the same local structure function method to analyze the 3-D structure taking the wind expansion effect into account.

In the present study, we perform the 3-D self-correlation function level contour analysis on the WIND spacecraft measurements. We construct the 3-D coordinate system using the mean magnetic field and the maximum variance fluctuation direction L obtained by MVA method. In section 2, we describe the data and methods used in order to study the 3-D anisotropy, including the way to construct the 3-D coordinate system and get the 3-D contour surfaces. We show our observational results in section 3. In section 4, we discuss our results and present our conclusions.

2. DATA AND METHOD

We use data from the Wind spacecraft during 14 years from 2005 to 2018, when the spacecraft hovers at the Lagrangian point $L1$ in the solar wind. The magnetic field investigation (Lepping et al. 1995) provides 3 s resolution magnetic field data, and, the three-dimensional plasma analyzer (Lin et al. 1995) measures the plasma data with a same cadence of $\Delta = 3$ s. We cut the data set into 1-hour intervals with no overlap and require that the data gap accounts for less than 5% in each interval. We remove the intervals with $\max[|\delta B_j|] < 2nT$, $\max[|\delta V_j|] < 20\text{km}$, where j indicates x, y, z axis in the geocentric-solar-ecliptic (GSE) coordinate system, and δ means the variation between every 3 s, in order to avoid the influence of shear magnetic field and shear flows.

For each interval i , we define the fluctuation as $\delta\vec{U} = \vec{U} - \bar{U}$, where \vec{U} is either magnetic field \vec{B} or velocity \vec{V} , and \bar{U} is obtained by performing a linear fit to \vec{U} . The two-time-point self-correlation function of $\delta\vec{U}$ is calculated as

$$R_U(i, \tau) = \langle \delta\vec{U}(t) \cdot \delta\vec{U}(t + \tau) \rangle, \quad (1)$$

here, $\tau = 0, \Delta, 2\Delta, \dots, 400\Delta$ is the time lag, and, $\langle \rangle$ denotes an ensemble time average. In order to easily make comparison, we use the zero time lag self-correlation $R(i, 0)$ to normalize the self-correlation function and obtain $R_{uu}(i, \tau) = R_U(i, \tau)/R(i, 0)$. In this way, the $R_{uu}(i, \tau)$ at $\tau = 0$ is always equal to 1. According to the Taylor hypothesis (Taylor 1938), we transfer the time lag to spatial lag using $r = \tau V_{\text{SW}}$, where r is the spatial lag and V_{SW} is the mean flow velocity in the corresponding interval i .

Wang et al. (2019) has shown the isotropic feature of the self-correlation level contours in a 2-D coordinate system. We extend this system to 3-D by introducing the maximum variance direction L , which is determined by performing minimum-variance analysis (MVA) method (Sonnerup & Cahill 1967) to the magnetic field data. This 3-D coordinate system uses the mean magnetic field \vec{B}_0 and the projection of maximum variance direction L in the plane perpendicular to the mean field as r_{\parallel} and $r_{\perp 2}$ components, respectively. $r_{\perp 1}$ components completes this orthogonal coordinate system. Any angles greater than 90° are reflected below 90° . In Figure 1, we show the angle θ_{VB} between the directions of V_{SW} and \vec{B}_0 and the angle ϕ_L between $r_{\perp 2}$ direction and the component of V_{SW} perpendicular to \vec{B}_0 for each interval i .

We find 23083 intervals in the slow solar wind ($V_{\text{SW}} < 400$ km/s) and 3347 intervals in the fast solar wind ($V_{\text{SW}} > 500$ km/s) and study their 3-D self-correlation level contours separately. The probability density function of θ_{VB} in the left panel of Figure 2 shows that the magnetic field is more oblique to the solar wind velocity in the slow wind than in the fast wind, which is consistent with the Parker Spiral theory. In the right panel, we show in the slow wind, there are more intervals with perpendicular ϕ_L than parallel ϕ_L , while the fast wind group has a roughly even distribution over 0° and 90° .

For each group, we bin θ_{VB} and ϕ_L into 15° bins and calculate the average of the normalized spatial self-correlation functions as follows:

$$R_{uu}(\theta_{\text{VB}}^m, \phi_L^n, r) = \frac{1}{n(\theta_{\text{VB}}^m, \phi_L^n)} \sum_{\substack{\theta_{\text{VB}}^n - 7.5 \leq \theta_{\text{VB}}(i) < \theta_{\text{VB}}^n + 7.5, \\ \phi_L^n - 7.5 \leq \phi_L(i) < \phi_L^n + 7.5}} R_{uu}(i, r) \quad (2)$$

where $n(\theta_{\text{VB}}^m, \phi_L^n)$ is the number of the intervals in corresponding bin, and, $\theta_{\text{VB}}^m = 15^\circ m + 7.5^\circ$; $\phi_L^n = 15^\circ n + 7.5^\circ$; $m, n = 0, 1, 2, \dots, 5$.

We obtain 36 averaged self-correlation functions for 36 $(\theta_{\text{VB}}, \phi_L) = 15^\circ \times 15^\circ$ bins. We analyze the contours at level $R_{uu}(\theta_{\text{VB}}, \phi_L, r) = 1/e \approx 0.368$, and obtain a r_{level} value by linear interpolation for each $(\theta_{\text{VB}}, \phi_L)$. In order to plot the contour surface in the 3-D coordinate system, we transform $(\theta_{\text{VB}}, \phi_L, r_{\text{level}})$ into $(r_{\perp 1}, r_{\perp 2}, r_{\parallel})$ by using $r_{\perp 1} = r_{\text{level}} \sin \theta_{\text{VB}} \sin \phi_L$, $r_{\perp 2} = r_{\text{level}} \sin \theta_{\text{VB}} \cos \phi_L$, $r_{\parallel} = r_{\text{level}} \cos \theta_{\text{VB}}$. We reflect the surface in the first octant into the other seven octants based on the assumption of reflectional symmetry. The result is presented in the next section.

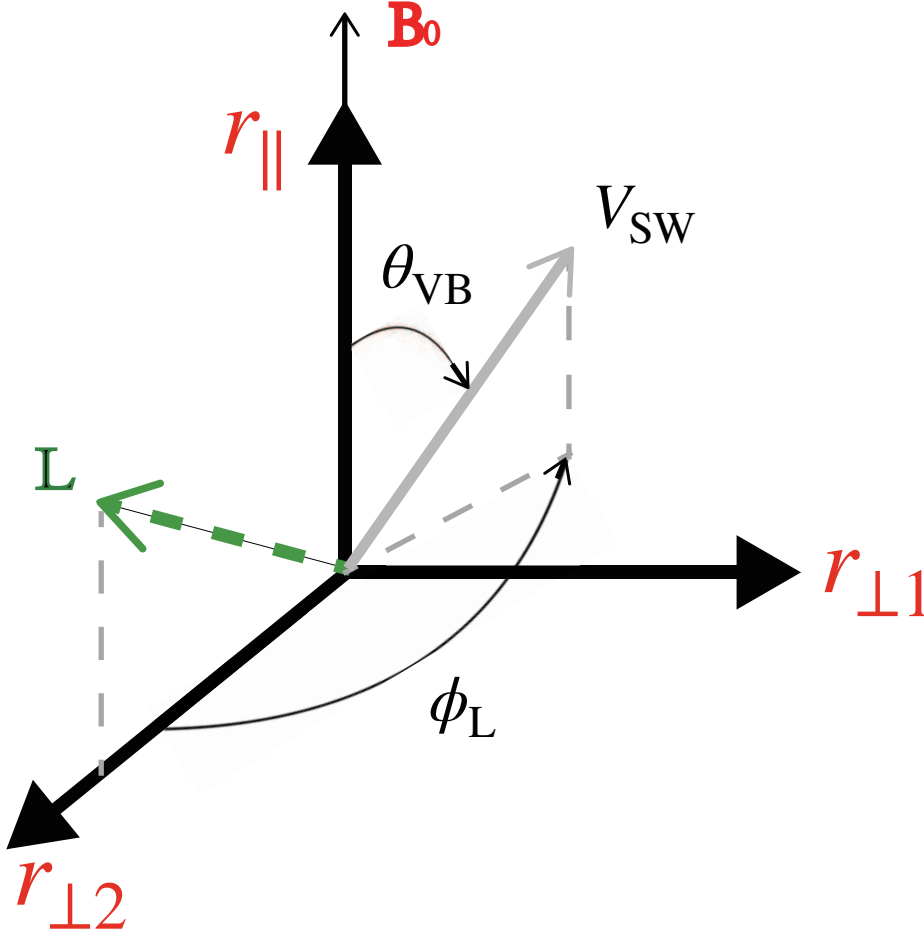


Figure 1. 3-D reference coordinate system used to compute correlation functions. For each 1-hour interval, r_{\parallel} corresponds to the direction of the mean magnetic field \vec{B}_0 , and, the projection of the maximum fluctuation direction L on the perpendicular plane is defined as $r_{\perp 2}$, and, $r_{\perp 1}$ completes this orthogonal coordinate system. θ_{VB} is the angle between the mean magnetic field and the solar wind velocity, and, ϕ_L is the angle between $r_{\perp 2}$ and the projection of the solar wind velocity on the plane perpendicular to \vec{B}_0 .

3. RESULTS

Figure 3 shows the averaged self-correlation functions in $r_{\perp 1}$, $r_{\perp 2}$, and r_{\parallel} directions, which correspond to the following angular bins:

$$r_{\perp 1} \rightarrow (75^\circ \leq \theta_{VB} \leq 90^\circ, 75^\circ \leq \phi_L \leq 90^\circ), \quad (3)$$

$$r_{\perp 2} \rightarrow (75^\circ \leq \theta_{VB} \leq 90^\circ, 0^\circ \leq \phi_L < 15^\circ), \quad (4)$$

$$r_{\parallel} \rightarrow (0^\circ \leq \theta_{VB} < 15^\circ, 0^\circ \leq \phi_L \leq 90^\circ). \quad (5)$$

In the left panel of Figure 3, we present the averaged magnetic self-correlation functions with standard error bars for both the slow solar wind (solid lines) and the fast solar wind (dashed lines). It is hard to distinguish the functions of the three directions for the slow wind. The phenomenon of the functions almost overlapping with each other means the 3-D isotropic feature of the self-correlation level contours in slow solar wind turbulence. For the fast wind, there is a slightly elongation along the $r_{\perp 2}$ direction in the perpendicular plane. Note that the magnetic self-correlation function of the fast wind is larger than that of the slow wind. When we consider self-correlation function with respect to the time lag instead of the spatial lag, the magnetic self-correlation functions for both the slow wind and the fast wind are almost the same (not shown). In the right panel, we show the averaged velocity self-correlation functions. They have

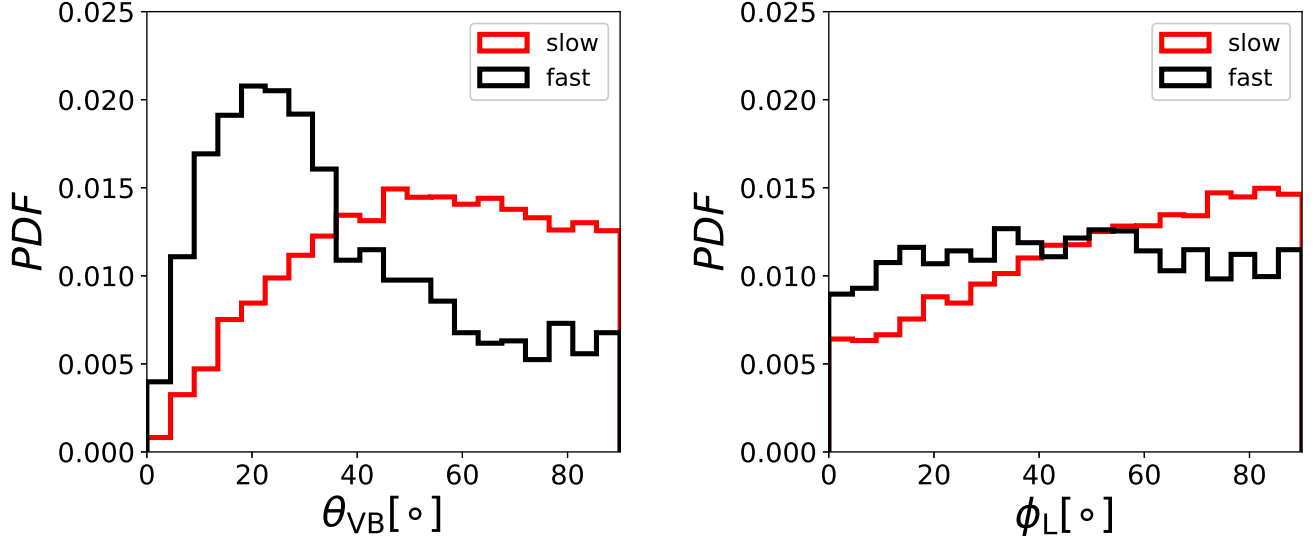


Figure 2. Probability density function of θ_{VB} (left) and ϕ_L (right). The red and black histograms are for the slow wind and the fast wind, respectively.

almost the same features as the averaged magnetic self-correlation functions except there is no clear elongation along the $r_{\perp 2}$ direction.

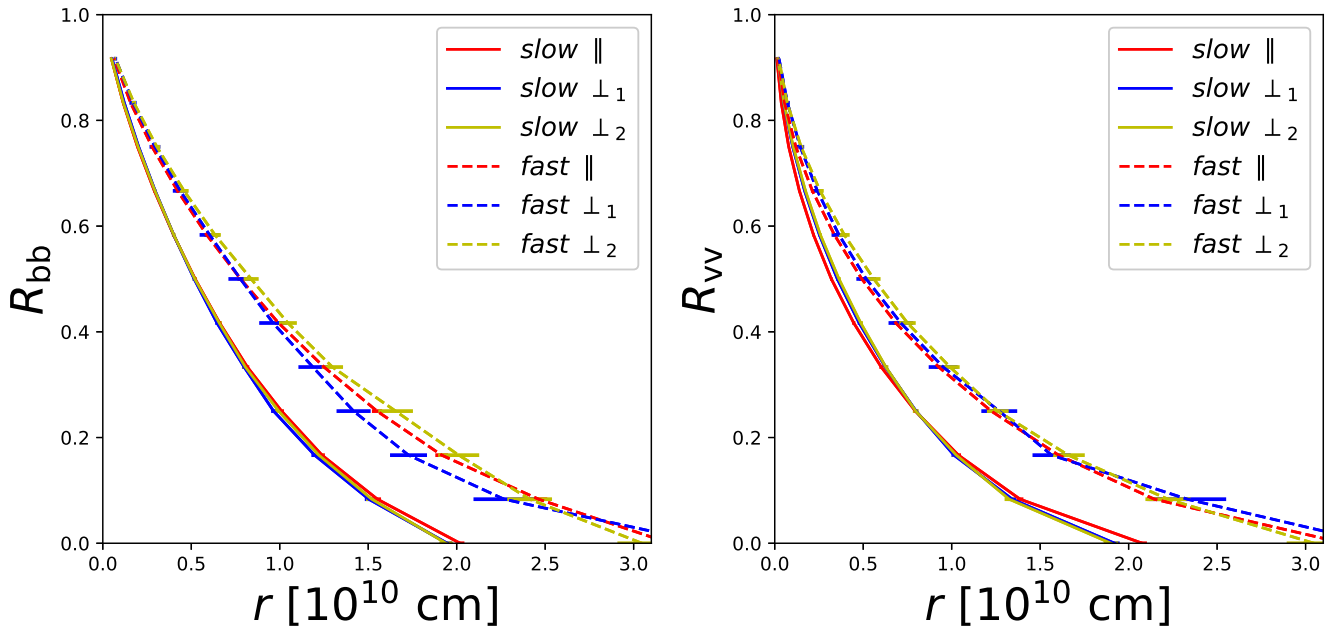


Figure 3. Left panel: Averaged normalized self-correlation functions $R_{bb}(r)$ of 1-hour-long magnetic field data. The solid and dashed lines are for the slow wind and the fast wind. Red, blue, and yellow colors correspond to the r_{\parallel} , $r_{\perp 1}$, and $r_{\perp 2}$ directions, respectively. The error bar shows the standard error of r_{level} for a given R_{bb} . Right panel: Averaged normalized self-correlation functions $R_{vv}(r)$ of 1-hour-long velocity data, in the same manner as the left panel.

We show the 3-D self-correlation level contour surfaces at level $R_{uu} = 0.368$ in Figure 4. In Figure 4(a), the slow wind magnetic field self-correlation function contour surface is almost a spherical surface. The projection closed curves

on the 2-D plane are plotted to help visualize the isotropic feature. They are almost round and almost identical to each other, which confirm the isotropic result. In Figure 4(b), the fast wind magnetic field self-correlation level contour surface departs a bit from a spherical surface. r_{level} in the $r_{\perp 2}$ direction is slightly longer. The projection closed curves on three planes are not round and have different sizes between each other. In Figure 4(c), the slow wind velocity field self-correlation level contour surface is almost spherical and the projection closed curves on the 2-D planes is also round and identical to each other, which shows a clear isotropic feature as the magnetic field. In Figure 4(d), the fast wind velocity field self-correlation level contour surface has a similar shape with that of magnetic field. The similarity between the magnetic field and velocity field contour shape supports the applicability of the data analysis technique here. We should also note that, the r_{level} is shorter for the slow wind than for the fast wind and shorter for the velocity field than for the magnetic field.

In order to evaluate the unevenness shown in Figure 4, we reduce the 3-D surface into the line trend with θ_{VB} and ϕ_{L} , as shown in Figure 5. We calculate the averaged r_{level} in 6 θ_{VB} bins from $0^\circ \leq \phi_{\text{L}} \leq 90^\circ$ with a weight of interval number in each ϕ_{L} bin. The result is shown in the left panel. We can clearly see that the variation with θ_{VB} is rather small for both the slow wind and the fast wind and for both the magnetic field and the velocity field. We calculate the average r_{level} in 6 ϕ_{L} bins from $60^\circ \leq \theta_{\text{VB}} \leq 90^\circ$ with a weight of interval number in the two θ_{VB} bins. The result is shown in the right panel. For the slow wind, the variation with ϕ_{L} is very small; while for the fast wind, there is a weak elongation along $r_{\perp 2}$. Again, it is easily seen that r_{level} is shorter for the slow wind and the velocity field.

In Figure 6, we show the variations with θ_{VB} and ϕ_{L} for the fast solar wind. The black solid and black dashed lines are the same as in Figure 5. We check the data intervals in the fast wind (group A) and further rule out the intervals with large gradient by visual inspection. We reserve 2272 cases (group B). The variations with θ_{VB} and ϕ_{L} for this new fast wind group B are calculated and shown in blue lines in Figure 6. The anisotropy for the fast group becomes weaker after we remove the structures more strictly.

4. DISCUSSION AND CONCLUSIONS

We present for the first time the 3-D self-correlation level contours of the magnetic field and the velocity field at 10^{10} cm scale based on WIND spacecraft measurements from 2005 to 2018. We construct a 3-D coordinate system according to the mean magnetic field direction and the maximum variance direction L of the magnetic field. The self-correlation contour surfaces at level $R_{uu} \approx 1/e$ in the slow solar wind are 3-D isotropic for both the magnetic field and the velocity field. The self-correlation contour surfaces at level $R_{uu} \approx 1/e$ in the fast solar wind show weak anisotropic feature in the perpendicular plane with an elongation along $r_{\perp 2}$. However, the anisotropy becomes weaker when we exclude the intervals with structures more strictly.

The 3-D coordinate system constructed here is consistent with the 3-D coordinate system presented by (Chen et al. 2012) if we consider the maximum variance direction L as the $(\vec{B}_1 - \vec{B}_2)$ in their work. Chen et al. (2012) present a structure function analysis in a scale-dependent 3-D coordinate system defined as follows: for each pair of points, the local mean field $B_{\text{local}} = (\vec{B}_1 + \vec{B}_2)/2$ was calculated as one axis and the local perpendicular fluctuation direction $B_{\text{local}} \times [(\vec{B}_1 - \vec{B}_2) \times B_{\text{local}}]$ as another axis. Verdini et al. (2018) perform a structure function analysis in the same 3-D coordinate system. However, our maximum variance direction L is based on the whole interval, while their local perpendicular fluctuation direction is adjusted for every two time instances.

The surfaces of the fast wind have an approximately 1.5 times larger spatial size than the surfaces of the slow wind for both the magnetic field and the velocity field. This result is consistent with the result of Wang et al. (2019). However, we also find that the correlation level contours are similar for the fast and slow wind without transferring the time lag into the spatial lag through the Taylor hypothesis. The reason why the fast wind has larger correlation level contour surfaces than the slow wind is unknown. The surfaces of the magnetic field have an approximately 1.3 times larger spatial size than the surfaces of the velocity field for both the fast wind and the slow wind. This result provides constraints for the solar wind turbulence theory.

The scale of 10^{10} cm corresponds more or less to the low-frequency break scale universally observed in the fast solar wind turbulence. The 3D quasi-isotropic feature of the self-correlation level contours in the fast solar wind is consistent with Figure 1 by Wicks et al. (2010) that the power spectrum is isotropic at the low-frequency break. Whether the anisotropy of the 3-D self-correlation level contours increase at smaller and smaller scales needs further study. That the contour of the velocity field is similar to the contour of the magnetic field is reasonable since magnetic and velocity fluctuations are coupled. Currently, we have no idea why the size of the magnetic contour is larger.

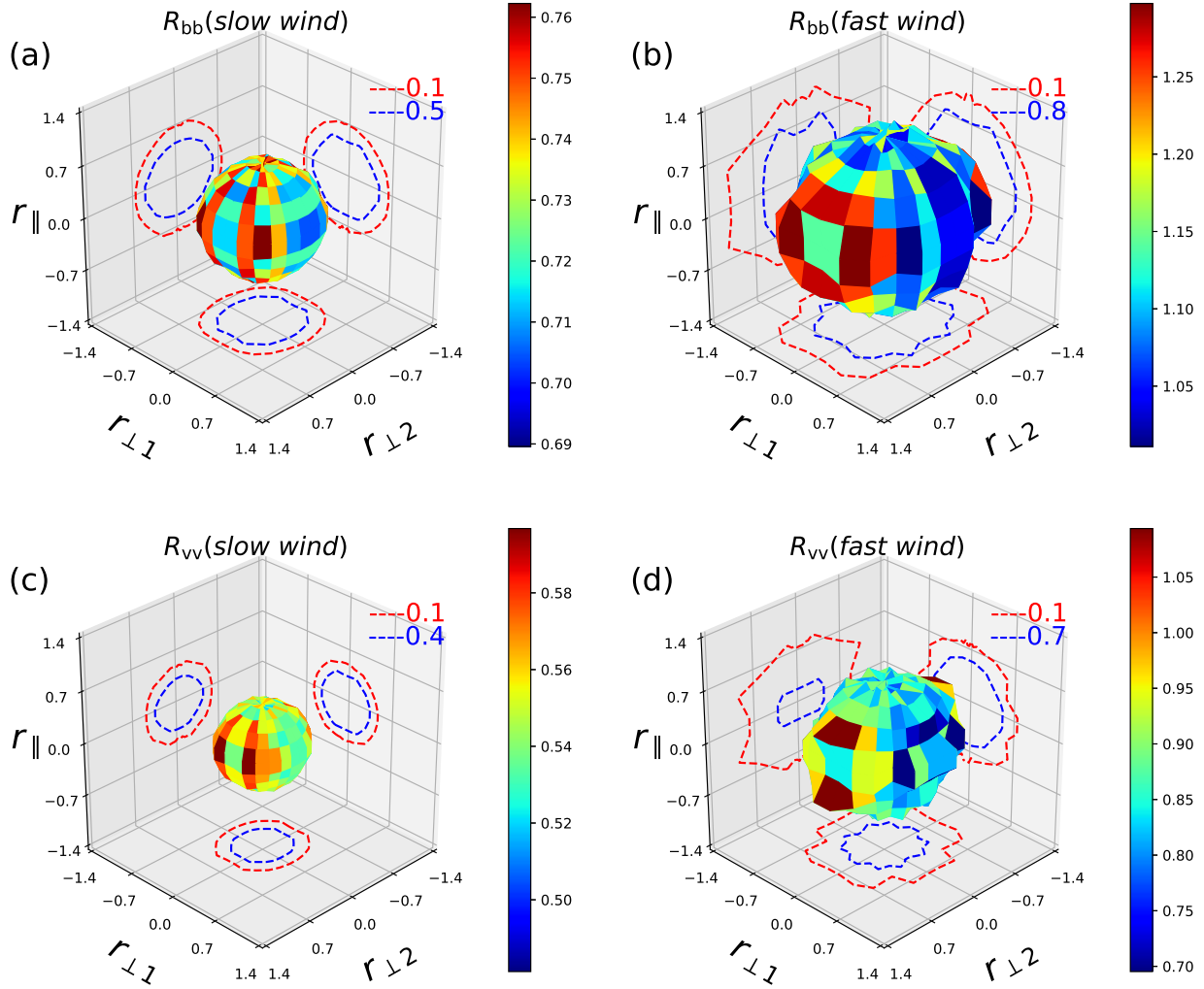


Figure 4. 3-D self-correlation level contour surface at level $R_{uu} = 0.368$ of (a) magnetic field in the slow wind; (b) magnetic field in the fast wind; (c) velocity field in the slow wind; (d) velocity field in the fast wind. The color represents r_{level} [10^{10} cm], which is the distances from the origin. The dashed red and blue lines in $r_{\perp 1} = -1.4$ plane are projections of the intersection lines of the surface with two planes $r_{\perp 1} = A1$ and $r_{\perp 1} = A2$, respectively, where $A1$ and $A2$ are shown in the legends with the corresponding colors in the corresponding panel; the dashed red and blue lines in $r_{\perp 2} = -1.4$ plane are projections of the intersection lines of the surface with two plane $r_{\perp 2} = A1$ and $r_{\perp 2} = A2$, respectively; the dashed red and blue lines in $r_{\parallel} = -1.4$ plane are projections of the intersection lines of the surface with two plane $r_{\parallel} = A1$ and $r_{\parallel} = A2$, respectively.

Recently, Bruno et al. (2019) find that the low-frequency break is also present in the slow solar wind magnetic spectra. They show a case with the break located around 10^{-4} Hz and an average velocity of 316 km/s. Our scale in the slow solar wind is smaller than the approximate break scale 3×10^{11} cm and is in the typical quasi-Kolmogorov range, as in Bruno et al. (2019). Our 3-D self-correlation level contour analysis of both the magnetic and velocity field shows a 3-D isotropic feature. We consider the self-correlation level contours represent the angular feature of the turbulence eddies. These results are not consistent with the predictions of the existed MHD theories. The 3-D isotropic feature of self-correlation level contour supports the Kolmogorov's theory (Kolmogorov 1941). How to interpret this result in the slow solar wind requires further investigation.

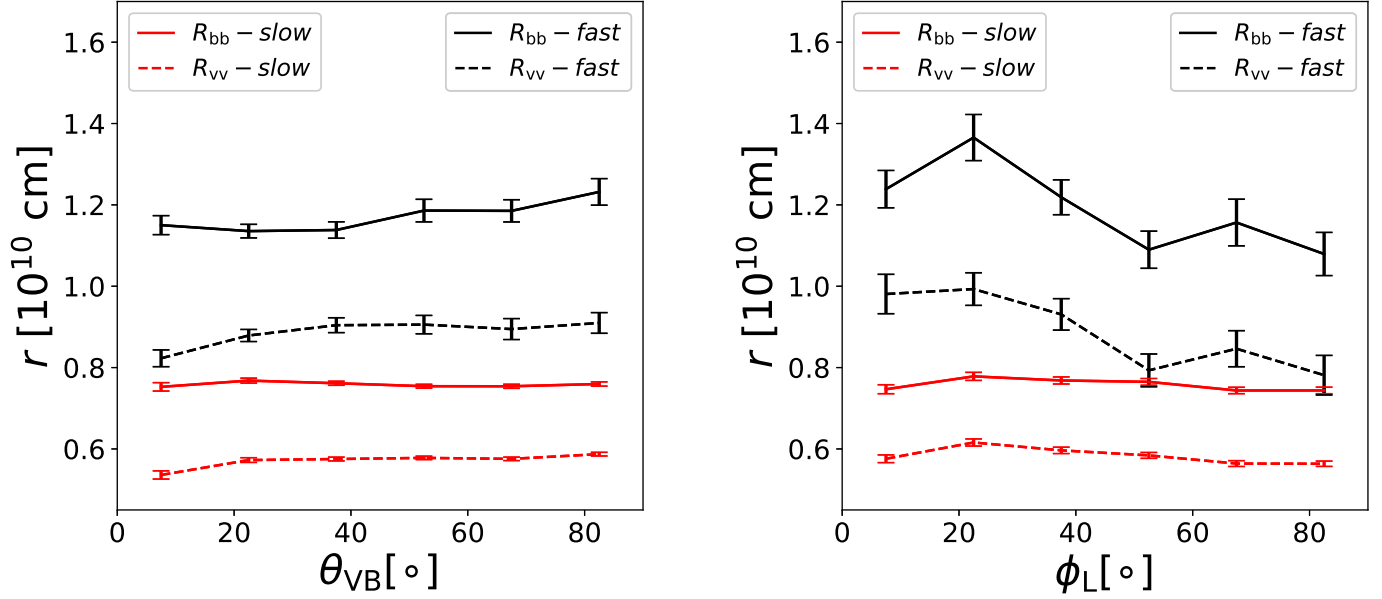


Figure 5. Left panel: averaged r_{level} in each θ_{VB} bin. The solid and dashed lines are for the magnetic field and the velocity field. And, the red and black lines indicate the slow wind and the fast wind, respectively. The error bars show the standard errors of the averaged r_{level} . Right panel: averaged r_{level} in each ϕ_{L} bin, in the same manner as the left panel.

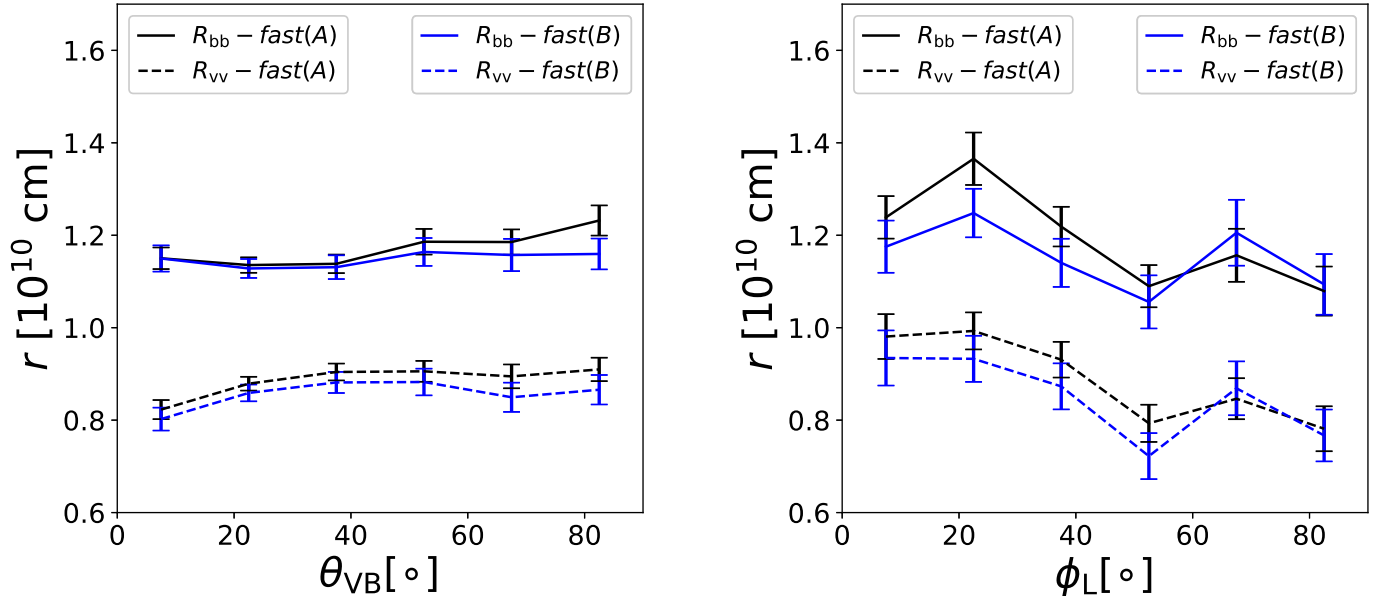


Figure 6. Left panel: averaged r_{level} in each θ_{VB} bin. The solid and dashed lines are for the magnetic field data and velocity data. And, the black and blue lines indicate the fast wind group A and the fast wind group B, respectively. The error bars show the standard errors of the averaged r_{level} . Right panel: averaged r_{level} in each ϕ_{L} bin, in the same manner as the left panel.

We thank the CDAWEB for access to the Wind data, Dr. Liping Yang and Dr. Junxiang Hu for helpful discussions. This work at Peking University and Beihang University is supported by the National Natural Science Foundation of China under contract Nos. 41474147, 41504130, 41874199, and 41674171.

REFERENCES

Boldyrev, S. 2006, Physical Review Letters, 96, 115002, doi: [10.1103/PhysRevLett.96.115002](https://doi.org/10.1103/PhysRevLett.96.115002)

Bruno, R., Telloni, D., Sorriso-Valvo, L., et al. 2019, A&A, 627, A96, doi: [10.1051/0004-6361/201935841](https://doi.org/10.1051/0004-6361/201935841)

- Chen, C. H. K., Horbury, T. S., Schekochihin, A. A., et al. 2010, *Phys. Rev. Lett.*, 104, 255002, doi: [10.1103/PhysRevLett.104.255002](https://doi.org/10.1103/PhysRevLett.104.255002)
- Chen, C. H. K., Mallet, A., Schekochihin, A. A., et al. 2012, *The Astrophysical Journal*, 758, 120
- Cho, J., & Vishniac, E. T. 2000, *The Astrophysical Journal*, 539, 273, doi: [10.1086/309213](https://doi.org/10.1086/309213)
- Dasso, S., Milano, L. J., Matthaeus, W. H., & Smith, C. W. 2005, *The Astrophysical Journal*, 635, L181, doi: [10.1086/499559](https://doi.org/10.1086/499559)
- Goldreich, P., & Sridhar, S. 1995, *Astrophys. J.*, 438, 763, doi: [10.1086/175121](https://doi.org/10.1086/175121)
- He, J., Tu, C., Marsch, E., Bourouaine, S., & Pei, Z. 2013, *Astrophys. J.*, 773, 72, doi: [10.1088/0004-637X/773/1/72](https://doi.org/10.1088/0004-637X/773/1/72)
- Horbury, T. S., Forman, M., & Oughton, S. 2008, *Physical Review Letters*, 101, 175005, doi: [10.1103/PhysRevLett.101.175005](https://doi.org/10.1103/PhysRevLett.101.175005)
- Kolmogorov, A. 1941, *Akademiia Nauk SSSR Doklady*, 30, 301
- Lepping, R. P., Acuña, M. H., Burlaga, L. F., et al. 1995, *Space Sci. Rev.*, 71, 207, doi: [10.1007/BF00751330](https://doi.org/10.1007/BF00751330)
- Lin, R. P., Anderson, K. A., Ashford, S., et al. 1995, *Space Sci. Rev.*, 71, 125, doi: [10.1007/BF00751328](https://doi.org/10.1007/BF00751328)
- Luo, Q. Y., & Wu, D. J. 2010, *The Astrophysical Journal*, 714, L138, doi: [10.1088/2041-8205/714/1/L138](https://doi.org/10.1088/2041-8205/714/1/L138)
- Matthaeus, W. H., Goldstein, M. L., & Roberts, D. A. 1990, *J. Geophys. Res.*, 95, 20673, doi: [10.1029/JA095iA12p20673](https://doi.org/10.1029/JA095iA12p20673)
- Oughton, S., Priest, E. R., & Matthaeus, W. H. 1994, *Journal of Fluid Mechanics*, 280, 95117, doi: [10.1017/S0022112094002867](https://doi.org/10.1017/S0022112094002867)
- Podesta, J. J. 2009, *Astrophys. J.*, 698, 986, doi: [10.1088/0004-637X/698/2/986](https://doi.org/10.1088/0004-637X/698/2/986)
- Shebalin, J. V., Matthaeus, W. H., & Montgomery, D. 1983, *Journal of Plasma Physics*, 29, 525, doi: [10.1017/S0022377800000933](https://doi.org/10.1017/S0022377800000933)
- Sonnerup, B. U. O., & Cahill, Jr., L. J. 1967, *J. Geophys. Res.*, 72, 171, doi: [10.1029/JZ072i001p00171](https://doi.org/10.1029/JZ072i001p00171)
- Taylor, G. I. 1938, *Proceedings of the Royal Society of London A: Mathematical, Physical and Engineering Sciences*, 164, 476, doi: [10.1098/rspa.1938.0032](https://doi.org/10.1098/rspa.1938.0032)
- Tu, C.-Y., & Marsch, E. 1995, *Space Sci. Rev.*, 73, 1, doi: [10.1007/BF00748891](https://doi.org/10.1007/BF00748891)
- Verdini, A., Grappin, R., Alexandrova, O., & Lion, S. 2018, *The Astrophysical Journal*, 853, 85, doi: [10.3847/1538-4357/aaa433](https://doi.org/10.3847/1538-4357/aaa433)
- Wang, X., Tu, C., & He, J. 2019, *The Astrophysical Journal*, 871, 93, doi: [10.3847/1538-4357/aaf64f](https://doi.org/10.3847/1538-4357/aaf64f)
- Wicks, R. T., Horbury, T. S., Chen, C. H. K., & Schekochihin, A. A. 2010, *Monthly Notices of the Royal Astronomical Society: Letters*, 407, L31, doi: [10.1111/j.1745-3933.2010.00898.x](https://doi.org/10.1111/j.1745-3933.2010.00898.x)